

## Key Points:

- Western Mediterranean deep layers were monitored in detail during the WMT at a key site near Minorca
- Evolution of the layered structure is analyzed in terms of double-diffusive mixing and ventilation
- Large heat and salt uptake of the deep Western Mediterranean was dominated by irregular renewals

## Supporting Information:

- Supporting Information S1
- Movie S1
- Movie S2

## Correspondence to:

S. Piñeiro,  
safo.pineiro@ieo.es

## Citation:

Piñeiro, S., González-Pola, C., Fernández-Díaz, J. M., & Balbin, R. (2019). Thermohaline evolution of the Western Mediterranean deep waters since 2005: Diffusive stages and interannual renewal injections. *Journal of Geophysical Research: Oceans*, 124, 8747–8766. <https://doi.org/10.1029/2019JC015094>

Received 25 FEB 2019

Accepted 13 AUG 2019

Accepted article online 17 AUG 2019

Published online 11 DEC 2019

The copyright line for this article was changed on 13 JAN 2020 after original online publication.

©2019. The Authors.

This is an open access article under the terms of the Creative Commons Attribution-NonCommercial-NoDerivs License, which permits use and distribution in any medium, provided the original work is properly cited, the use is non-commercial and no modifications or adaptations are made.

# Thermohaline Evolution of the Western Mediterranean Deep Waters Since 2005: Diffusive Stages and Interannual Renewal Injections

S. Piñeiro<sup>1</sup> , C. González-Pola<sup>2</sup> , J. M. Fernández-Díaz<sup>3</sup>, and R. Balbin<sup>1</sup> 

<sup>1</sup>Instituto Español de Oceanografía, Centro Oceanográfico de Baleares, Palma, Spain, <sup>2</sup>Instituto Español de Oceanografía, Centro Oceanográfico de Gijón, Gijón, Spain, <sup>3</sup>Department of Physics, Universidad de Oviedo, Oviedo, Spain

**Abstract** A large production of anomalous dense water in the northwestern Mediterranean Sea during winter 2005 led to a widespread abrupt shift in Western Mediterranean deep waters characteristics. This new configuration, the so-called Western Mediterranean Transition (WMT), involved a complex thermohaline structure that was tracked over time through a deep hydrographic station located NE of Minorca Island, sampled 37 times between 2004 and 2017. In this study, the thermohaline evolution of the WMT signal is analyzed in detail. Using a 1-D diffusion model sensitive to double-diffusive mixing phenomena, the contribution to the heat and salt budgets of the deep Western Mediterranean in terms of ventilation and diffusive transference from the intermediate layers above is disentangled. Results show distinct stages in the evolution of the deep waters, driven by background diffusion and intermittent injections of new waters. The progression of a multilayered structure in the deep ocean is well represented through existing parameterizations of salt fingering and diffusive layering processes and makes it possible to infer an independent estimate of regional background diffusivity consistent with current knowledge. Overall, the deep layers of the Western Mediterranean underwent substantial warming (0.059 °C) and salt increase (0.021) between 2004 and 2017, mostly dominated by injections of dense waters in the 2005–2006 and 2011–2013 periods. Thus, within the WMT period, heat uptake rate in the deep Western Mediterranean was substantially higher than that of the intermediate levels in the global ocean.

## 1. Introduction

Ocean ventilation is a fundamental piece in Earth's heat redistribution dynamics and hydrological cycle. Winter buoyancy loss of surface waters in dense-water formation areas is the main mechanism driving the ventilation of the ocean interior and modulating heat storage below the permanent thermocline. For this reason, areas prone to deep convection activity are hot spots for the study of ocean circulation and climate (Marshall & Schott, 1999; Winton et al., 2013).

The northwestern Mediterranean Sea is one of the few active dense-water formation areas outside the polar regions (MEDOC Group, 1970). The area is characterized by a wind-driven cyclonic circulation that induces the uplift of isopycnals. Winter northerly cold and dry winds blow over the region in violent bursts enhancing evaporation and cooling and, therefore, causing surface layers to lose buoyancy and sink. Inside the cyclonic gyre (Figure 1a), the doming of the isopycnals favors winter vertical mixing between the surface Atlantic Water (AW) and the intermediate levels beneath occupied by the Levantine Intermediate Water (LIW), formed in the Eastern Mediterranean. This results mainly in salinification of the former and, accordingly, a further reduction in vertical stability. At interannual scales, intense surface buoyancy loss during extreme winters can trigger mixing to reach deep waters and even the ocean bottom, transferring heat and salt downward from the LIW and giving rise to the Western Mediterranean Deep Water (WMDW). The WMDW spreads over the whole Western Mediterranean (WMED; Rhein, 1995) and eventually contributes to the characteristics of the Mediterranean Outflow Water (MOW; García-Lafuente et al., 2009). Concurrent with this open-sea process, distinct dense-water formation occurs over the shelf of the Gulf of Lions (GoL; Figure 1a) with intermittent recurrence. These dense waters cascade through submarine canyons and contribute to the newly formed WMDW characteristics (Canals et al., 2006).

During winter 2005 a large production of anomalous dense water led to a widespread abrupt shift in WMDW characteristics (Font et al., 2007; López-Jurado et al., 2005; Salat et al., 2007; Schroeder et al., 2006). This

event, the so-called Western Mediterranean Transition (WMT; Schroeder et al., 2016) induced drastic changes in the classical vertical structure of the deep waters and disrupted the smooth progressive salinification and warming trends detected in the twentieth century.

Since its formation, the evolution of the WMT has been tracked and studied directly or indirectly by different projects and monitoring programs, from the formation area in the GoL to the Algerian basin (e.g., Durrieu de Madron et al., 2013; Houpert et al., 2016; Puig et al., 2013; Schroeder et al., 2009, 2013; Schroeder et al., 2016; Waldman et al., 2016). The conspicuous signature that emerged after winter 2005 has progressively eroded, resulting in much warmer, salty waters that currently fill the deep layers of the WMED. Several projects carried out by the *Instituto Español de Oceanografía* and grouped nowadays under the RADMED (*RADiales del MEDiterráneo*) monitoring program (López-Jurado et al., 2015) have been gathering hydrographic data on a seasonal basis along the Spanish Mediterranean coast since the late 1990s. The deep stations included in this program provide a detailed picture of the evolution of the WMT along the eastern continental slope of the Iberian Peninsula, midway between the WMDW origin at the GoL and the Alboran Sea.

In this study, the thermohaline evolution of the WMT signal, its fade and subsequent deep-water renewal variability are analyzed in detail using hydrographic data from a station located NE of Minorca Island. A 1-D diffusion model sensitive to double-diffusive mixing phenomena is used in order to obtain the theoretical diffusive evolution of the  $\theta$ - $S$  profiles. This numerical approach enables us to disentangle the contribution to the heat and salt budgets of the deep WMED in terms of ventilation due to the advection of dense waters injected in the formation area and the diffusive transfer of heat and salt from the intermediate layers above.

The paper is organized as follows. The data set is presented in section 2. In section 3, the processing applied to the hydrographic data is explained and the diffusion model scheme is described in detail. In section 4, the obtained results are exposed, and these are subsequently discussed in section 5. Lastly, final conclusions and considerations are presented in section 6.

## 2. Data Set

The Minorca deep station (40°10.00'N, 04°34.96'E, 2,540 m deep) is a deep hydrographic station located on the outer continental slope included in the sampling strategy of the RADMED monitoring program (López-Jurado et al., 2015; Figure 1a). This station, located outside the dense-water formation area, is a privileged site since the continental slope of the Balearic Islands is the preferential advective pathway of the newly formed deep waters toward the Algerian basin (Beuvier et al., 2012) and also of the cascading waters (Durrieu de Madron et al., 2013). Through the RADMED surveys and other projects in support, it was occupied 37 times from 2004 to early 2017 (Figure 1b). It offers a comprehensive view of the temporal variability of the thermohaline changes induced by the WMT and the subsequent intermittent injections of dense waters in the formation region (Figure 1c). This hydrographic time series was obtained by means of an SBE 911plus CTD (conductivity-temperature-depth) installed on an SBE 32 carousel water sampler (occasionally SBE 25 or SBE 19plus). Instrument calibration and cast processing were performed following standard protocols as described in López-Jurado et al. (2015).

The thermohaline signature of the different water masses present below 300 dbar in the WMED is easily identifiable in the  $\theta$ - $S$  diagram (Figure 1c). The warm and salty LIW core is located between 300 and 600 dbar, followed by a transition region with a smooth stratification where salinity ( $S$ ) and potential temperature ( $\theta$ ) decrease with depth toward the WMDW core at the bottom of the basin. The complex thermohaline structure that emerged in winter 2005 modified this classical vertical structure and created a hook-shaped  $\theta$ - $S$  profile in the deep waters due to the appearance of a saltier and warmer new deep water mass (nWMDW) beneath the old WMDW (oWMDW) and a cascading-origin fresher and colder water at the bottom (cWMDW; López-Jurado et al., 2005; Puig et al., 2009; Salat et al., 2007; Schroeder et al., 2006; see notations in Figure 1c). Even though thermohaline anomalies in the deep layers of the WMED have been observed previously (as bottom increments of  $\theta$  and  $S$  or even complete hook-like features; Bethoux & Tailliez, 1994; Bethoux et al., 2002; Lacombe et al., 1985; Puig et al., 2013; Salat et al., 2009), the large input of dense water in 2005 created an unprecedented structure hundreds of meters thick that triggered a large uplift of the isopycnals over the whole basin (Schroeder et al., 2008) causing the appearance of an

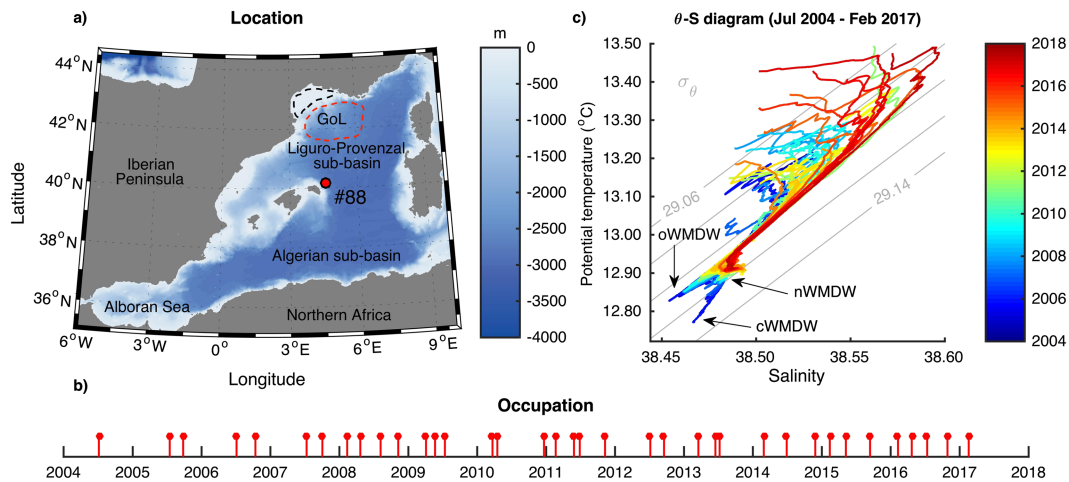


**Figure 1.** (a) Location of the RADMED #88 deep station (red dot). Red dashed line shows the open-ocean deep water formation area, and the black dashed line shows the cascading-origin dense waters formation area as stated in Houpert et al. (2016). (b) Occupation from 2004 to 2017. (c)  $\theta$ -S diagram from 300 dbar to the bottom from July 2004 to February 2017. Gray lines denote isopycnal levels ( $\sigma_\theta$ ) every  $0.02 \text{ kg/m}^3$ . WMDW = Western Mediterranean Deep Water. RADMED = 'RADiales del MEDiterráneo'.

interface between the oWMDW and the nWMDW at about 1,000 dbar above the bottom (clearly identifiable in Figure 1c).

### 3. Methodology

This study focuses on the relative role of diffusion versus advection of dense waters in the long-term thermohaline evolution of the deep waters at the Minorca station during the WMT period. To address the issue, the output of the theoretical diffusive evolution of the water column from a 1-D model is compared with the actual 12-year hydrographic time series. Divergences between observations and the model are then attributed to lateral advection of ventilated dense waters from the formation area in the GoL. This approach treats local observed profiles as the result of decoupled advection and diffusion, which is an approximation of a much more complex 3-D process in which the advected water column mixes vertically while spreading, strongly conditioned by background shear. The idealized 1-D diffusive evolution requires assumptions regarding diffusive coefficients values and its vertical structure that have to be based on current knowledge of ocean mixing processes while being consistent with the local observed evolution. The limitations of what the 1-D model can represent, that is, spatial heterogeneity in mixing and spreading cannot be taken into account, should be kept in mind when discussing the outcomes.

Since raw hydrographic time series have a noisy character, a necessary first step is to construct a smoothed version of the hydrographic evolution. Then, a brief description of the diffusive processes expected in the deep waters of the WMED within the WMT configuration is provided, followed by a description of the procedure for the numerical treatment of such a diffusion process.

#### 3.1. Smoothed Evolution of the Hydrography

Preprocessing of the raw hydrographic record is required to obtain a smooth evolution of the WMT structure. Filtering of natural noise due to mesoscale or higher frequency processes is not straightforward, since the vertical and temporal scales are not comparable and time series are not evenly sampled. While different approaches could be followed, this specific study only required a reasonable smooth temporal variation of the hydrographic structure to be achieved; therefore, a simple approach was applied as described below.

Discarding the surface layer (0–300 dbar), the 37  $\theta$ -S profiles were first stabilized to remove small scale density inversions using the algorithm described in Barker and McDougall (2017) and included in the TEOS-10 software (IOC, SCOR & IAPSO, 2010). Then a digital filter with a 50-dbar window was applied to remove small-scale structures below such a range. Since five profiles did not reach the bottom (see section 4), the vertical structure of the closest profile (in time) was used to interpolate the time series matrix. Finally, a locally estimated scatterplot smoothing (LOESS; Seifert & Gasser, 2004) was used as a smoother for

the temporal variation of  $\theta$  and  $S$ , making it possible to obtain continuous time series at each pressure level encompassing the period between 15 July 2005 and 12 February 2017 (section 4). A fortnightly series of profiles was then extracted. Vertical stability of the interpolated profiles was carefully examined to verify that there were no spurious density inversions larger than the instrument resolution ( $10^{-4}$  kg/m<sup>3</sup>) due to the data treatment. Further checks indicated that the LOESS smoother applied here is similar to a third order Butterworth digital filter (Emery & Thomson, 2001) with a cutoff frequency of 12–18 months, adequate to remove intra-annual noise and to maintain the signal of interannual injections of dense waters. The LOESS approach was preferred since it is less sensitive to outliers, mainly present in the interface region.

A comparison between the smoothed and original profiles can be observed in Movie S1 in the supporting information. Root-mean-square deviation between raw and smoothed time series can be considered as indicative of the intrinsic noise of the data set. Hereafter this smoothed time series will be considered as the observational record.

### 3.2. Turbulent Diffusion and Double-Diffusive Mixing Parameterization

In the absence of ventilation, the water column structure generated by the WMT should evolve by diapycnal mixing, mostly accomplished by transient turbulent motions induced by dynamical instabilities such as internal wave breaking or current shear (Klymak & Nash, 2009). By analogy with molecular fluxes, turbulent fluxes of heat and salt are commonly parameterized by Fickian diffusion. Thus, following Fick's second law, vertical ( $z$ ) temporal ( $t$ ) diffusive evolution of the thermohaline properties ( $c$ ) of the water column in Minorca can be straightforwardly estimated in terms of the tracer gradient and an eddy diffusion coefficient ( $K_c$ ; Klymak & Nash, 2009). In one dimension,

$$\frac{\partial c}{\partial t} = \frac{\partial}{\partial z} \left( K_c(z) \frac{\partial c}{\partial z} \right). \quad (1)$$

General circulation models usually approach diapycnal mixing assuming same depth-dependent  $K_c$  for both scalars ( $S$  and  $\theta$ ; e.g., Jayne, 2009). However, under certain thermohaline configurations of the water column (both  $\theta$  and  $S$  decreasing or increasing with depth) asymmetries may arise between  $\theta$  and  $S$  diffusion coefficients due to the difference in heat and salt molecular diffusivity. This so-called double-diffusive mixing (Kelley et al., 2003; Radko, 2013; Schmitt, 2009) can become of great importance if turbulence is not strong because it may greatly vary both  $K_\theta$  and  $K_S$  and transfer heat and salt unequally.

During the WMT, the vertical thermohaline structure in the Minorca deep station appears to be favorable for both forms of double-diffusion: salt fingering (warmer salty waters over colder and fresher ones) and diffusive layering (cold and relatively fresh waters over warmer and saltier ones; Bryden, Schroeder, Borghini, et al., 2014). The warm and salty LIW overlying the fresher and colder WMDW is a permanent feature of the basin, causing salt fingering instabilities to be operating transporting salt downward more efficiently than heat. Its main fine-scale signature, the thermohaline staircases (Schmitt, 1994), has been observed repeatedly in this region and seems to be a ubiquitous feature throughout the Algerian and Tyrrhenian subbasins (Bryden, Schroeder, Borghini, et al., 2014; Bryden, Schroeder, Sparnocchia, et al., 2014; Durante et al., 2019; Johannessen & Lee, 1974; Zodiatis & Gasparini, 1996). Additionally, the injection of anomalous warm and salty dense waters during the WMT created a transition region between the oWMDW and the nWMDW prone to diffusive layering, known to transfer heat upward more efficiently than salt. Similarly, the deepest region of the water column, between the nWMDW and the cWMDW, became a region prone to salt fingering.

In order to identify where double-diffusive mixing processes are operating in the water column, the reference parameter is the local density ratio  $R_\rho = (\alpha T_z)/(\beta S_z)$  (Turner, 1973), where  $T_z$  and  $S_z$  are the vertical gradients of temperature and salinity and  $\alpha$  and  $\beta$  are the thermal expansion and haline contraction coefficients of seawater, respectively. Under static stability, the condition for double diffusion is  $R_\rho > 0$  and its intensity depends, besides  $R_\rho$  value, on the Lewis number ( $\tau = \kappa_T/\kappa_S$ ), where  $\kappa_T$  and  $\kappa_S$  are the molecular diffusivities of heat and salt. Salt fingering is active when  $1 < R_\rho < \tau \approx 100$ , whereas diffusive layering requires  $1 > R_\rho > \tau^{-1} \approx 0.01$  (Kelley et al., 2003; Schmitt, 2009).

Both forms of double diffusion are more active and have a major impact on diapycnal mixing when  $R_\rho$  approaches one (Schmitt, 1994). In this study, large-scale  $K_\theta$  and  $K_S$  under these mixing regimes are

estimated following  $R_\rho$ -dependent parameterizations used in Zhang et al. (1998) and Zhang and Schmitt (2000), which evaluate diffusivities as a separate contribution of double-diffusive mixing added to constant background mixing. Accordingly, for the salt fingering regime,

$$K_S = \frac{K^*}{1 + (R_\rho/R_c)^n} + K^\infty \quad \text{and} \quad K_\theta = \frac{0.7K^*}{R_\rho[1 + (R_\rho/R_c)^n]} + K^\infty, \quad (2)$$

where  $K^* = 2 \times 10^{-4} \text{ m}^2/\text{s}$  is the maximum salt finger diffusivity,  $R_c = 1.6$  is the critical density ratio above which salt-finger-driven diffusivities decrease abruptly,  $n = 6$  controls the drop of  $K_\theta$  and  $K_S$  regarding the increment of  $R_\rho$ , and  $K^\infty$  is the constant diapycnal diffusivity due to background mixing related to intermittent dynamical instabilities and not to double diffusion.

For the diffusive layering regime, Zhang et al. (1998) parameterize  $K_\theta$  and  $K_S$  according to the empirical formulations of Kelley (1984, 1990) but with minor modifications to address both forms of double diffusion and to represent the effects of background turbulence:

$$K_\theta = CR_a^{1/3}\kappa_T + K^\infty \quad \text{and} \quad K_S = R_F R_\rho (K_\theta - K^\infty) + K^\infty, \quad (3)$$

where

$$C = 0.0032 \exp(4.8R_\rho^{0.72}) \quad R_a = 0.25 \times 10^9 R_\rho^{-1.1} \quad R_F = \frac{1/R_\rho + 1.4(1/R_\rho - 1)^{3/2}}{1 + 14(1/R_\rho - 1)^{3/2}}$$

and

$$\kappa_T = 1.4 \times 10^{-7} \text{ m}^2/\text{s}.$$

For regions where the water column is doubly stable for both  $S$  and  $\theta$  (no double diffusion), a classical turbulence parameterization is adopted to represent the background mixing induced by transient dynamical instabilities:

$$K_\theta = K_S = K^\infty. \quad (4)$$

It should be noted that the general vertical structure of the WMED is prone to double-diffusive regimes and the doubly stable portions of the water column are a minority and, generally, transient.

The same parameters as used in Zhang and Schmitt (2000) are adopted here. As opposed to Zhang et al. (1998), who discard double-diffusion in the deep layers, no constraint to the double-diffusion activity is applied. Indeed, regions prone to both forms of double diffusion can be found in the deep waters of the Mediterranean (Meccia et al., 2016; Onken, 2003).

$K_{S,\theta}(z)$  values (both under double-diffusive regimes and not) can be found in the literature inferred from analytical studies or derived from field observations (e.g., Kunze & Toole, 1997; Ledwell et al., 1993, 1998, 2000; Polzin et al., 1997; Schmitt et al., 2005; Schmitt & Ledwell, 2001; Schmitt et al., 2005; St. Laurent & Schmitt, 1999; St. Laurent et al., 2001; Toole et al., 1994). As described below, specific periods where the evolution of the profiles is consistent with pure diffusion were used here to estimate an optimal  $K^\infty$  local value.

### 3.3. Numerical Integration of the Diffusion Equation

The basis of this study was the comparison between the actual evolution of the deep ocean hydrography and what would be caused by pure diffusion alone. Therefore, it was necessary to integrate the diffusion equation numerically given some boundary conditions and a  $K_{S,\theta}(z)$  parameterization; that is, it was necessary to set up a simple 1-D diffusion model. The setting was as follows:

The vertical coordinate ( $z$ ) was discretized regularly on a vertical grid of  $n$  points and height  $H$ , with a resolution of  $\delta z = H/n$ . At each time step ( $\delta t$ ), mixing regimes throughout the water column were identified by means of the Turner angle (Ruddick, 1983) and  $K_\theta$  and  $K_S$  profiles were estimated following the  $R_\rho$ -dependent parameterizations previously described (section 3.2).

The one-dimensional diffusion equation (1) was solved numerically for both  $\theta$  and  $S$  using a Crank-Nicolson scheme (second-order implicit; Crank & Nicolson, 1947), with  $\delta t = 2.4$  hr and  $\delta z = 10$  m (chosen to secure numerical stability while allowing quick runs). The domain ranged from 800 dbar, well below the influence of the LIW core fluctuations, to 2,420 dbar. Simulations started with an observed profile from the smoothed set.

Density is used here as a diagnosis variable. Since evolution of  $\theta$  and  $S$  is considered independently, it is in principle possible to create spurious density inversions invalidating the simple diffusion scheme. Finally, this was not the case in any of the simulations so no convective adjustment scheme for unstable stratification regions was required.

To close the scheme, two boundary conditions were set. At the seafloor it is assumed that there is no flux (i.e., a Neumann condition  $\partial c/\partial z = 0$  at  $z = H$ ). This is obvious for salinity and can be arguable for temperature due to geothermal heating, as discussed below.

Conditions at the upper boundary of the domain were set by the  $\theta$  and  $S$  values and their vertical gradient at the thermohalocline, inferred from the observed profiles below the LIW core. These values change over time, modulating the heat and salt fluxes toward deeper layers. To include this time varying boundary condition, an assimilation scheme was applied that replaced, at each  $\delta t$ , the upper domain of the profile with a combination of the simulated profile and the observed profile in such a way that the top of the simulation matched the observations, imposing continuity in the profile and its gradient (Figure 2). The assimilation was performed above an isopycnal level slightly lighter than the bottom limit of the oWMDW, ensuring that the heat and salt fluxes transferred by downward diffusion into the WMT structure were modulated by the actual hydrographic record but never altering the anomaly. An isopycnal level was preferred rather than a fixed isobaric level because it integrates changes in the vertical position of the structures due to heave effects (Bindoff & McDougall, 1994). Further details concerning the numerical assimilation can be found in Appendix A. Movie S2 in the supporting information illustrates the process.

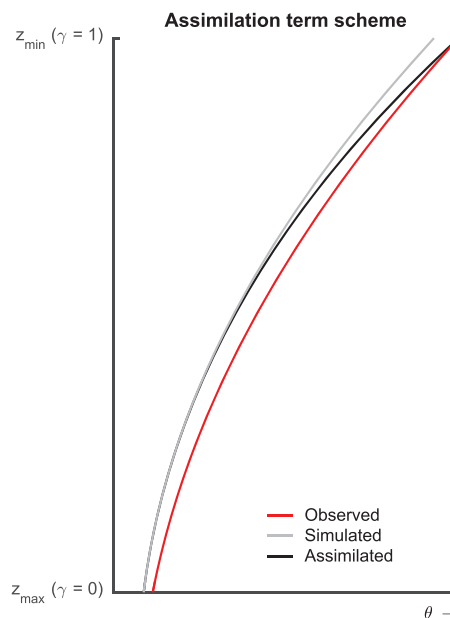


**Figure 2.** Assimilation term scheme used in the 1-D diffusion model. Two  $\theta$  profiles are shown: the simulated one (gray) and the one inferred from the observations (red) at that particular moment of the time series. The resulting profile (black) is a combination of both.  $z_{\min}$  refers to the upper limit of the domain (800 dbar) and  $z_{\max}$  to the assimilation limit, which in turn corresponds to the pressure of the heaviest isopycnal that always remains above the oWMDW-nWMDW interface. For further details on nomenclature and formulation, the reader is referred to Appendix A. WMDW = Western Mediterranean Deep Water.

### 3.4. $K^\infty$ Local Estimation

Due to the nearly seasonal frequency sampling, it is possible to look for periods within the overall 12 years when the thermohaline evolution had a clear purely diffusive behavior. An estimate of  $K^\infty$  can be inferred from such periods. In order to identify these, certain criteria were followed: (i) no appearance of new isopycnals at the bottom, (ii) no large doming of isopycnals in the time series that could indicate lateral advection at intermediate depths, (iii)  $\theta$ - $S$  profile maxima and minima erosion over the period, and (iv) no bibliographic evidence of deep convection in the formation area within the period.

Over the periods identified as diffusive,  $\theta$  and  $S$  differences between the model and the observations were computed. Since both variables were measured simultaneously and had different ranges of variation in the water column, the error of the two measurements can be normalized by dividing each measure ( $c_i$ ) by the standard deviation ( $\sigma_c$ ) after subtracting the mean ( $\bar{c}$ ), that is,  $Z(c)_i = (c_i - \bar{c})/\sigma_c$ . Therefore, a combined normalized root-mean-square error (RMSE) can be defined:

$$\text{RMSE}_{\theta S}^{\text{nor}} = \sqrt{\frac{1}{2} \left( \frac{1}{n} \sum (Z(\theta)_{\text{mod}} - Z(\theta)_{\text{obs}})^2 + \frac{1}{n} \sum (Z(S)_{\text{mod}} - Z(S)_{\text{obs}})^2 \right)}. \quad (5)$$

A locally estimated optimum  $K^\infty$  can be obtained by minimizing  $\text{RMSE}_{\theta S}^{\text{nor}}$  from an exhaustive inspection of  $K^\infty$  over realistic ranges in the simulations of markedly diffusive periods.

## 4. Results

### 4.1. $\theta$ - $S$ Shape Evolution

The local thermohaline evolution of the deep waters in Minorca is roughly governed by continuous diffusive mixing and water renewals by irregular inputs. Considering the shape of the  $\theta$ - $S$  diagrams in the deep layers (Figure 3), it can be noticed that since the event that gave rise to the WMT, different waters with specific signatures were injected at interannual scales. Advection of these new waters to Minorca caused an enhancement of the thermohaline gradients and the appearance of new structures in the  $\theta$ - $S$  plane that distorted the initial signature of the WMT.

Three main stages in the evolution of the deep waters can be distinguished from the hydrographic data: first, a hook-shaped stage from July 2005 to presumably December 2010 (since the CTD did not reach the bottom depth) corresponding to the appearance of the initial WMT structure and the consequent interface between the oWMDW and the nWMDW at about 1,200 dbar. Within this period, after winter 2006, the production of deep water seems absent or not relevant for the evolution of the new deep waters, which appear to be dominated by diffusive mixing processes. The cascading waters and the  $\theta$ - $S$  maximum associated with the nWMDW were progressively eroded. In 2009, a small disturbance appeared at the bottom and established

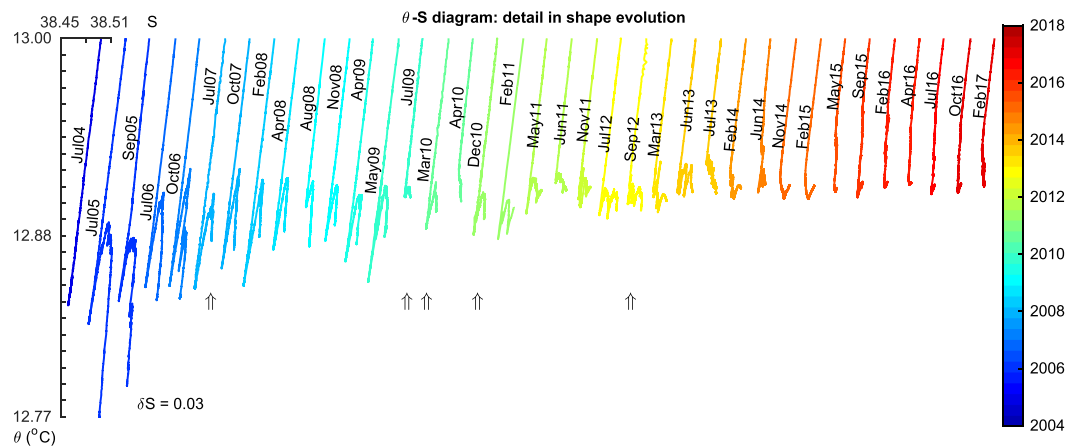


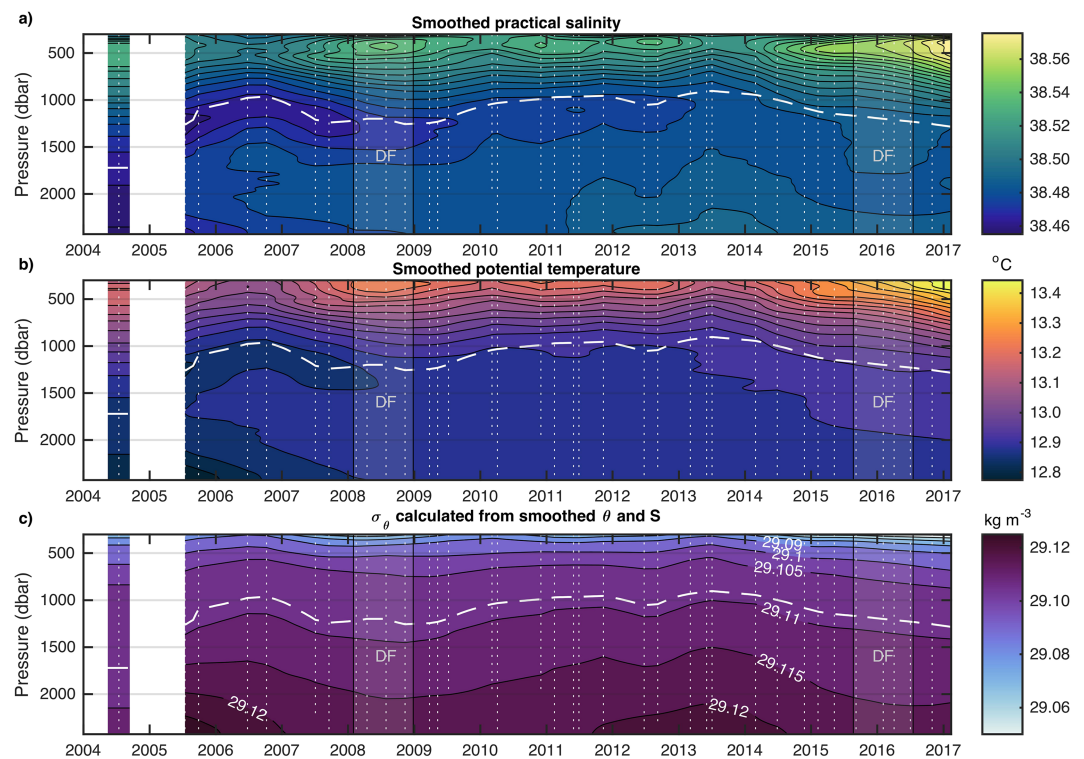
**Figure 3.** Detail in shape evolution of the  $\theta$ - $S$  diagram below the LIW core in Minorca. Axes refer to the 2004 profile. Subsequent profiles are shifted in time by  $\delta S$ . Arrows indicate the profiles that did not reach the bottom depth. LIW = Levantine Intermediate Water.

the beginnings of the second stage, defined by a more complex  $m$ -shaped  $\theta$ - $S$  structure, ranging from 2010 to 2014. Several major deep-water formation events occurred within this period (see section 5.1). From November 2014 to February 2017, without evidence or report of large-scale convective events, the  $\theta$ - $S$  profile turned into an  $V$ -shape, defining the third stage.

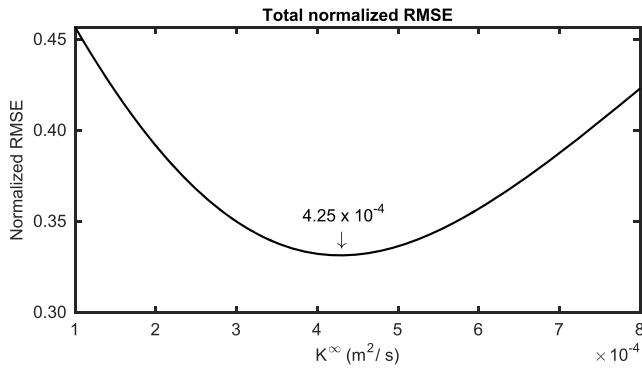
#### 4.2. Best Estimate of $K^\infty$

Figure 4 shows contours of the smoothed observational records where short-term and small-scale variations were filtered (see also supporting information). A key portion of the water column is the oWMDW-nWMDW interface created by the WMT, clearly visible in the contours as a salinity minimum starting around 1,200 dbar (Figure 4a). This interface remains traceable until around mid-2014, when the structure of the deep waters is strongly eroded. By inspection, the  $\sigma_\theta = 29.1088 \text{ kg/m}^3$  isopycnal (white dashed line in Figure 4) was selected as the reference level closest to the oWMDW-nWMDW interface, since it always remained above it throughout the entire time series. This isopycnal was taken as the limit of assimilation in the simulations and the maximum pressure reached was 1,280 dbar. This pressure was later used as a reference to compute changes in the heat and salt budgets of the deep waters within the WMT.

Potential density anomaly ( $\sigma_\theta$ ) contour corroborates what was anticipated by the analysis of the  $\theta$ - $S$  profiles shape, showing the occurrence of new density levels at the bottom and a generalized uplift of the isopycnals in the whole water column in the two periods characterized by the presence of anomalous structures below 1,000 dbar, 2005–2006 and 2009–2013 (Figure 4c). Within the a priori diffusive periods inferred from the observed profiles (Figure 3), the hook-shaped stage after 2006 and the  $V$ -shaped stage, two periods that met the criteria established in section 3.4 were selected to infer a local estimate of  $K^\infty$ : the first one, from 15 February 2008 to 26 December 2008 (315 days); and the second one, between 6 September 2015 and 2 July 2016 (300 days). Both periods, highlighted in Figure 4, include four observed profiles each.



**Figure 4.** (a) Smoothed  $S$ , (b)  $\theta$ , and (c)  $\sigma_\theta$  evolution between July 2005 and February 2017 in Minorca from 300 to 2,420 dbar. July 2004 profile is included for reference. The white dashed line indicates  $29.1088 \text{ kg/m}^3$  isopycnal pressure. Highlighted boxes delimitate the diffusive periods (DF) where local  $K^\infty$  was estimated. Vertical white dotted lines indicate the date of each conductivity-temperature-depth cast and their maximum pressure reached.



**Figure 5.** Total normalized RMSE for the two diffusive periods between the simulations and the observational record for simulations with  $K^\infty \in (1 \times 10^{-4} \text{ m}^2/\text{s}, 8 \times 10^{-4} \text{ m}^2/\text{s})$ . RMSE = root-mean-square error.

Since the periods have substantially similar time intervals, giving equal weight to both, the  $\text{RMSE}_{\text{OS}}^{\text{nor}}$  were combined and a minimum in  $K^\infty = 4.25 \times 10^{-4} \text{ m}^2/\text{s}$  was obtained (Figure 5). This value minimizes the differences between the simulations of both periods and the observational record. Roughly speaking,  $K^\infty \in (3.5 \times 10^{-4} \text{ m}^2/\text{s}, 5.5 \times 10^{-4} \text{ m}^2/\text{s})$  is consistent with the observed evolution of the purely diffusive stages. Taking the combined optimized  $K^\infty$ , specific simulations for each period yield maximum  $\theta$  differences of  $10^{-3} \text{ }^\circ\text{C}$  and  $<10^{-3}$  for  $S$ .

### 4.3. The 2005–2017 Simulations: Long-Term Single Runs

In order to evaluate what the degradation of the WMT structure would be like if only diffusion were present, two 12-year simulations were carried out using 15 July 2005 as the initial profile (i.e., the profile in which the anomaly was observed for the first time). Every 15 days an output profile was obtained from the simulation, enabling a comparison with the fortnightly observational record. In the first simulation, the assimilation term

was not included; that is, the initial  $\theta$  and  $S$  values at the upper boundary (800 dbar) were kept constant, thus allowing the thermohalocline below to evolve freely by diffusion. The second simulation included the assimilation term up to the indicated 29.1088 isopycnal pressure, forcing the thermohalocline to evolve toward observations (see Figure 6 and Movie S2 in the supporting information). As indicated, the inclusion of assimilation modulates the downward transference of heat and salt from intermediate layers by taking into account their actual evolution.

In both simulations, the initial Turner angle profiles show a complex interleaved succession of mixing regimes throughout the water column derived from the WMT structure. As expected, mixing near the

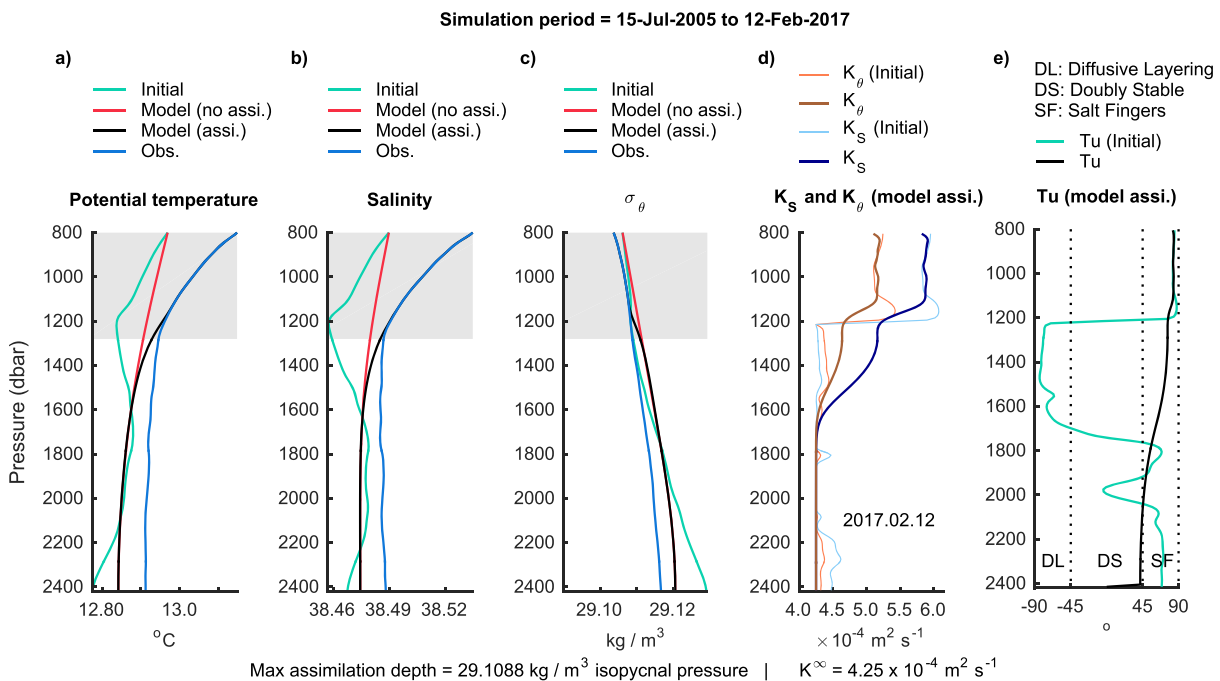


**Figure 6.** (a)  $\theta$  profile evolution between July 2005 and February 2017 (800–2,420 dbar). Initial profile (turquoise line) and observed (blue line), simulated without assimilation (red line) and simulated with assimilation (black line) profiles in February 2017. (b) Same as (a) but for  $S$ . (c) Same as (a) and (b) but for  $\sigma_\theta$ . Shaded areas indicate the maximum assimilation pressure range during the simulation. (d)  $K_\theta$  (brown line) and  $K_S$  (dark blue line) simulated profiles with assimilation in February 2017.  $K_\theta$  (thin orange line) and  $K_S$  (thin light blue line) profiles correspond to the July 2005 initial profile. (e) Turner angle profile in February 2017 simulated with assimilation (black line) and July 2005 initial profile (turquoise line). Dotted vertical lines delimit the three mixing regimes (see Ruddick, 1983). To observe the complete simulation, the reader is referred to Movie S2 in the supporting information.

bottom in the transition region between the cWMDW and the nWMDW core presents salt finger activity of moderate intensity ( $Tu \approx 69^\circ$ ) with some enhancement of diffusive coefficients from background values (up to  $K_\theta \approx 4.3 \times 10^{-4} \text{ m}^2/\text{s}$  and  $K_S \approx 4.5 \times 10^{-4} \text{ m}^2/\text{s}$ ), thus salt is transported downward more efficiently than heat. In the transition region between the nWMDW core and its interface with the oWMDW, diffusive layering is operating ( $Tu \approx -81^\circ$ ) transporting heat upward more efficiently than salt ( $K_\theta \approx 4.4 \times 10^{-4} \text{ m}^2/\text{s}$  and  $K_S \approx 4.3 \times 10^{-4} \text{ m}^2/\text{s}$ ). Above the interface, at the base of the thermohalocline, the mixing regime returns to salt finger activity that is much stronger than at the deepest levels ( $Tu \approx 87^\circ$ ), yielding values up to  $K_\theta \approx 5.4 \times 10^{-4} \text{ m}^2/\text{s}$  and  $K_S \approx 6 \times 10^{-4} \text{ m}^2/\text{s}$  (Figures 6d and 6e).

As the structures erode, transitions between the different water masses are subjected to weaker gradients and hence the intensity of double-diffusion below the interface decreases. By mid-2008, the transition region above nWMDW core reverses its  $\theta$  gradient, halting diffusive layering. By the end of 2011, regions prone to double diffusion below 1,600 dbar are no longer detected. As the profiles evolve and the WMT degrades, the influence of the salt fingers of the thermohalocline deepens until reaching a maximum at about 1,700 dbar by the end of the simulation. Strictly speaking, in 2017 there are areas prone to salt fingers down to 2,000 dbar but salinity gradients are so weak that salt fingering instabilities cannot develop to effectively influence the eddy diffusion coefficients (Figures 6d and 6e).

Differences between simulations (with and without assimilation) are subtle at the interface and the water masses beneath are degraded in the same fashion (Figure 6). By 2011 only a cold-haline tongue is perceptible in the deepest part of the  $\theta$ - $S$  diagram as a remnant of the WMT (see Movie S2 in the supporting information). At the end of the simulation in 2017 the WMT signature is barely perceptible; its erosion is practically complete (Figures 6 and 7a).

After 12 years of simulation, a comparison between the modeled diffusive evolution and the observational record highlights a large deficit of heat and salt in the deep waters (Figures 6a, 6b, and 7). The origin of this deficit is irretrievably water renewal, that is, lateral advection. To evaluate the relative contribution of both terms (diffusive transference from the intermediate layers and lateral advection) to the evolution of heat (QC) and salt contents (SC) in the deep layers, budgets were calculated for the simulated time series and for the observed profiles below 1,280 dbar (Figures 7b and 7c).

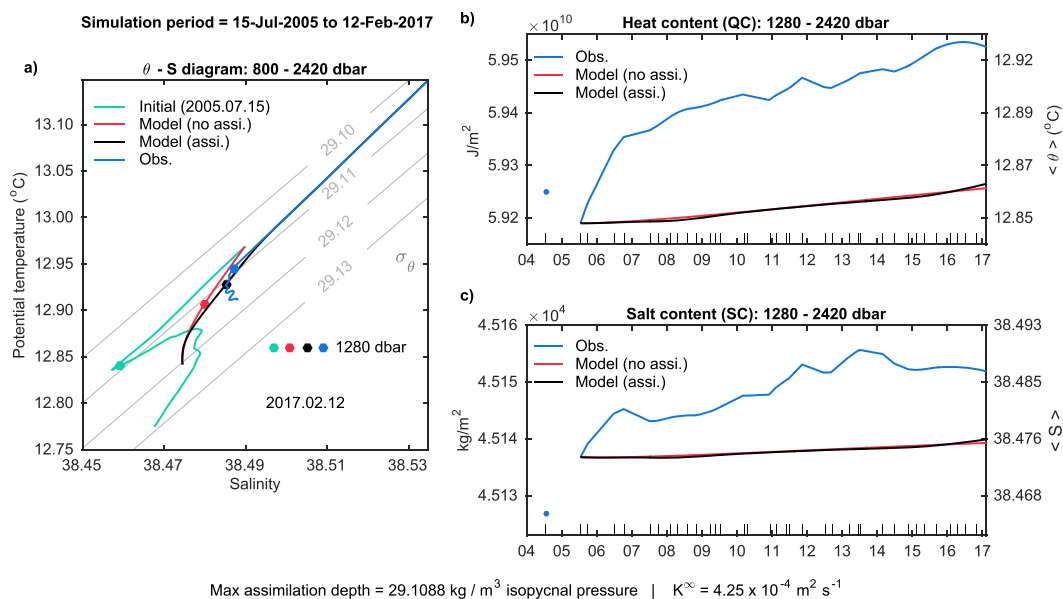


**Figure 7.** (a)  $\theta$ - $S$  diagram evolution between July 2005 and February 2017 (800–2,420 dbar); initial profile (turquoise line) and modeled with assimilation (black line), modeled without assimilation (red line), and observed (blue line) profiles in February 2017. Dots indicate the maximum assimilation pressure (1,280 dbar). Gray lines denote isopycnal levels ( $\sigma_\theta$ ). (b) QC evolution between July 2005 and February 2017 (1,280–2,420 dbar) in the model with assimilation (black line), in the model without assimilation (red line), and in the observed profiles (blue line). (c) Same as (b) but for SC. QC and SC in 2004 (1,280–2,420 dbar) are included in (b) and (c) for reference (blue dot). Thin vertical lines on the x axis in (b) and (c) indicate the date of the conductivity-temperature-depth casts. Corresponding  $\langle \theta \rangle$  and  $\langle S \rangle$  changes of the layer were obtained as  $\bar{\theta} = QC / (\bar{\rho} C_p V)$  and  $\bar{S} = SC / (\bar{\rho} V)$ .  $C_p = 3,926 \text{ J} \cdot \text{kg}^{-1} \cdot ^\circ\text{C}^{-1}$ ,  $\bar{\rho} = 1,029 \text{ kg/m}^3$ , and  $V = 1,140 \text{ m}^3$ .

On the whole,  $QC$  and  $SC$  in the deep layers evolved similarly in both simulations (with and without assimilation), with slight differences due to the thermohaline assimilation. As the gradients of the deep regions weakened, transfer of heat and salt through the thermohaline expanded the extension of the salt fingering influence. Therefore, after 2008, as the thermohaline structure of the WMT faded from the  $\theta$ - $S$  diagram,  $QS$  and  $SC$  began to increase more rapidly (Figures 7b and 7c)

$QC$  and  $SC$  below 1,280 dbar calculated from the observed profiles showed that, after the 2005–2006 large increase, the deep layers continued to gain heat and salt in a fairly progressive manner over time, showing swings attributed to injections of differentiated advected waters. Between 2005 and 2017,  $\theta$  and  $S$  of the deep layers (below 1,280 dbar) rose by  $0.073\text{ }^{\circ}\text{C}$  and  $0.013$ , respectively. This represents an increase in the  $QC$  and  $SC$  of  $3.35 \times 10^8\text{ J/m}^2$  and  $15.10\text{ kg/m}^2$ . Heat uptake of this portion of the water column within the period was  $\dot{Q} = 0.92\text{ W/m}^2$ . The diffusive heat transfer from the thermohaline as estimated from the model runs was  $\dot{Q} = 0.21\text{ W/m}^2$ , that is, 22%, leaving 78% to lateral advection. In the case of salt,  $3.13\text{ kg/m}^2$  was transferred from the intermediate layers between 2005 and 2017, representing 21% of the observed increments. An estimate of the relative contribution of background diffusion and double diffusion to  $\dot{Q}$  and  $\dot{S}$  can be inferred from specific model runs evaluating separately both terms. If double diffusion is discarded, downward heat and salt fluxes are reduced by 8% and 21%, respectively, for the whole period. The greatest advective contribution of heat and salt occurred in the first years after the onset of the anomaly. Around half of the  $QC$  and  $SC$  was injected between 2005 and 2006. After such a period, the relative importance of the diffusive transference through the thermohaline to the heat and salt budgets of the deep layers increased to around 40%.

#### 4.4. The 2005–2017 Simulations: Restarting Runs by Observations

In order to evaluate the interannual evolution of heat and salt advection, short-term simulations were carried out starting on the dates when the station was occupied (i.e., starting on the actual profiles that determine the smoothed fortnightly time series). After evolving by diffusion to the next actual observed profile, differences in  $QC$  and  $SC$  were estimated (Figure 8) and grouped annually to obtain the time series of advected heat and salt budgets (Figure 9). Due to the irregular sampling frequency, it was not possible to specify when advected water actually arrived between years and it was assumed a smooth progression between

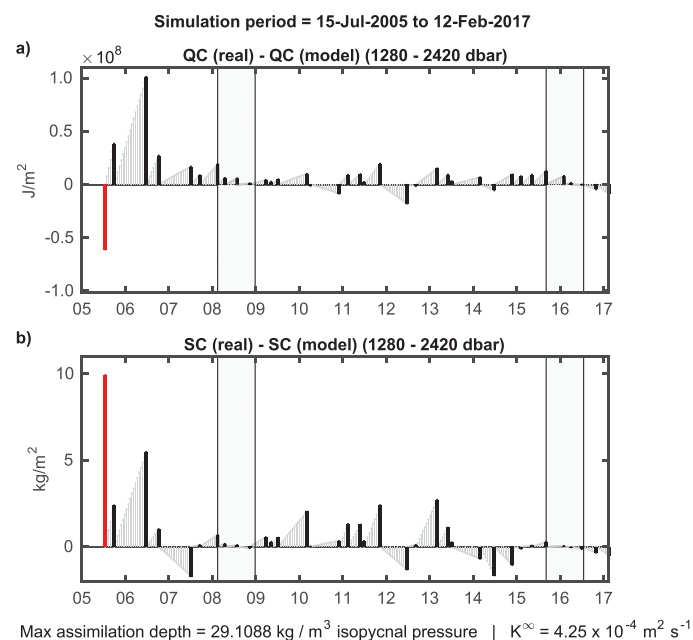


**Figure 8.** (a)  $QC$  differences between the observations and the model 2005–2017 (1,280–2,420 dbar; gray bars). (b)  $SC$  differences between the observations and the model 2005–2017 (1,280–2,420 dbar; gray bars). Black bars are the differences between the observations and the model at model runs restart. The red bars in 2005 include the differences between 2004 and 2005. Highlighted boxes delimit the periods in which  $K^{\infty}$  was estimated.

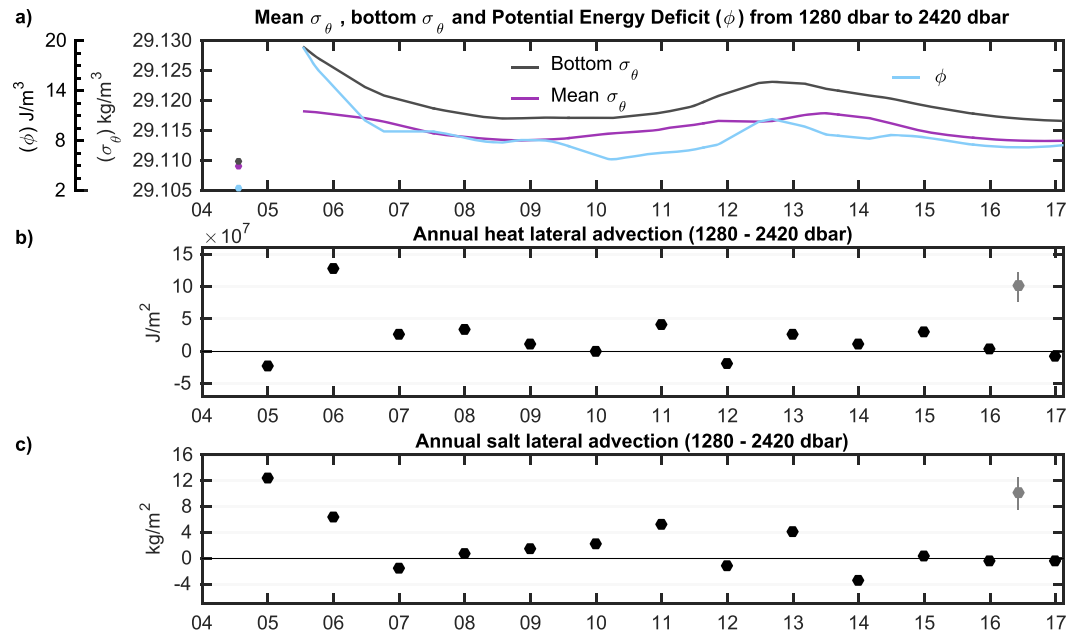


**Figure 9.** (a) Mean  $\sigma_\theta$  (purple line), bottom  $\sigma_\theta$  (black line) and potential energy deficit ( $\phi$ ; blue line) evolution in the observed profiles 2005–2017 (1,280–2,420 dbar). The 2004 values are included (purple, black, and blue dots). (b) Annual heat lateral advection evolution 2005–2017 (1,280–2,420 dbar). (c) Annual salt lateral advection evolution 2005–2017 (1,280–2,420 dbar). Error bars are included in (b) and (c) (upper right corner, in gray) for reference (see section 4.4).

consecutive occupations. RMSE between the *QC* ( $RMSE_{QC} = 2.29 \times 10^7 J/m^2$ ) and *SC* ( $RMSE_{SC} = 2.5 kg/m^2$ ) computed from the smoothed time series and the actual observations may be considered an intrinsic error estimate for the observational record in terms of annually advected heat and salt and are included in Figure 9 as error bars (in gray) for reference.

As expected, the best fit between observed and modeled heat-salt evolution is found in the periods previously regarded as diffusive and chosen to infer  $K^\infty$  (highlighted boxes in Figure 8), especially in the case of salt. It is worth noting that the first markedly diffusive period starts on 15 February 2008, and over 60% of annual heat advection in 2008 (Figure 9b) occurred prior to this date.

To assess the changes caused by the advection of ventilated waters in the density structure, the average  $\sigma_\theta$  and the potential energy deficit (de Boer et al., 2008; Planque et al., 2006) of the layer were computed, as well as the  $\sigma_\theta$  at 2,240 dbar (Figure 9a).

## 5. Discussion

The existence of the Minorca hydrographic station regularly occupied since the WMT formation enables a detailed view of the evolution of the anomaly at a key site that complements our current knowledge of this event. The signature of yearly renewals of deep waters in the basin and their relevance in terms of heat and salt content evolution is discussed in this section. Moreover, we address how the formation and free evolution of a multilayered structure with a sharp interface provides insights into the mixing behavior of the deep waters.

### 5.1. Interannual Contribution of Lateral Advection Versus Vertical Diffusion

Assessment of diffusive heat and salt fluxes through the thermohalocline provided by the model enables us to infer the contribution to the *QC* and *SC* of the deep waters due to lateral advection. These contributions provide information on the characteristics of the newly formed deep water along its passage across the NE of Minorca toward the Algerian basin. In practice, if any of the locally observed properties (salt or heat) diverge from what would be consistent with purely diffusive evolution, advection of new waters should be present. Lack of such divergence may be assumed as indicative of the absence of advection, although strictly speaking

this is not certain since arrival of waters with the same hydrographic signature would yield no signal. Estimates of deep-water formation rate and properties can be found in the bibliography from observational data and models. This enables us to understand the tracking of changes as seen at the Minorca station. The sequence is as follows.

From the inventory of annual heat and salt advective component (Figures 9b and 9c), it was observed that the onset of the WMT in winter 2005 entailed the largest advective contribution to the salt content of the deep layers on record. In contrast, despite the nWMDW being markedly warmer than oWMDW, heat content below 1,280 dbar was reduced in 2005 due to the presence of very cold cascading-origin waters (Canals et al., 2006; Font et al., 2007). The water column above the newly created interface also cooled due to the generalized uplift of the oWMDW (López-Jurado et al., 2005; Zunino et al., 2012). The cold fresh cascading waters signature progressively vanished within a year, likely due to the combination of its erosion due to mixing and its continued advection toward the deepest part of the basin. The following year, 2006, nWMDW was again created and the formation area extended to the Ligurian Sea (Schroeder et al., 2008; Smith et al., 2008; Somot et al., 2018; Zunino et al., 2012) but cascading events were much less prominent (Fuda et al., 2009; Puig et al., 2013). Large amounts of heat and salt were incorporated into the water column in 2006 (Figures 9b and 9c) in agreement with observations at the DYFAMED site (Schroeder et al., 2010).

No deep convective events were reported in the MEDOC formation area in the two following years, 2007 and 2008 (Houpert et al., 2016; Puig et al., 2013; Schroeder et al., 2013). Local balances at Minorca suggest salt loss in 2007 (below estimated uncertainty) and heat gain in 2007 and 2008, in the latter mostly gathered at the beginning of the year. We interpret this outcome as the progressive rearrangement of the water column after the two convective years 2005–2006. 2007–2008 evolution implied a reduction in density, that is, consistent with leakage of denser (colder) water toward deeper areas of the basin.

In 2009 and 2010 deep-water formation events were reported in the GoL (Houpert et al., 2016; Fuda et al., 2009; Schroeder et al., 2013) as well as minor cascading events (Puig et al., 2013). The hindcast simulation of Somot et al. (2018) identified 2009 as strongly convective, but small advective contributions were detected off Minorca, especially in terms of salt (Figures 9b and 9c). New thermohaline structures in the deep layers emerged in the GoL region in 2010 (Houpert et al., 2016; Puig et al., 2013) and by 2011 the signature in the Minorca station was prominent.

From 2011 to 2013, moderate to intense deep-water formation events were reported in the GoL (Durrieu de Madron et al., 2013; Houpert et al., 2016; Puig et al., 2013; Schroeder et al., 2013; Waldman et al., 2016). The record at Minorca shows that within the period 2011–2013 almost as much salt as in 2005 was incorporated into the deep layers. The 2012 case, a remarkably cold winter in the Mediterranean (Chiggiato et al., 2016; Durrieu de Madron et al., 2013; Houpert et al., 2016; Somot et al., 2018), is notable since it is the only one showing cooling + freshening signature. The newly formed WMDW along with the dense cascading water formed that year occupied the deepest part of the basin underlying the resident deep waters (Durrieu de Madron et al., 2013) thus causing the complete development of the *m*-shape in the  $\theta$ -*S* diagram characteristic of the 2011–2013 convective period. Accordingly, 2012 shows a bottom density maximum and an increase in stratification of the deep layers that reflect the dense cascading signal and the appearance of such a complex structure. In 2013, an intense deep water formation event occurred again (Houpert et al., 2016; Waldman et al., 2016), but no cascading signal was detected. This event was the subject of detailed observational and modeling studies presented in *Journal of Geophysical Research-Oceans* and *Journal of Geophysical Research-Atmospheres* special issues (Conan et al., 2018). After this period no further convective events were reported except for one of minor intensity in 2015 (Durrieu de Madron et al., 2017).

The years following 2013 revealed salt loss (2014) and heat gain (mostly 2015). This sequence partially resembles the postconvection stages after the WMT onset in 2005, despite the very different water column structures emerging after both events. A year with extreme cascading (2005 and 2012) was followed by a year with large deep convection but weaker or absent cascading (2006 and 2013). A year later, salt loss was observed (2007 and 2014) and further gain of heat followed next (early 2008 and 2015). Density dropped smoothly throughout the process (2005–2008; 2012–2015). The overall sequence is consistent with the arrival of signatures of newly formed waters at time scales within a year or less, followed by a more complex transient stage which involves further leakage of denser portions of the water column. The salinity drop

in both cases—2007 and 2014—is mostly driven by sinking of the salinity minimum at the oWMDW-nWMDW interface. The last years of the series—2016 and 2017—showed a stable water configuration consistent with further diffusive erosion of the remnants of the structures.

Continuous tracking of changes at the Minorca station provides a complementary record that, being consistent with current knowledge of deep-water formation events, adds insights regarding transient postconvective stages and propagation time scales across the basin. Overall balance indicates that  $\approx 80\%$  of the heat and salt injected into the water column disturbed by the WMT anomaly came from ventilation. It is worth noting that warming and salting through the thermohalocline is not a process that ought to occur at a homogeneous rate across the basin. Indeed, studies of the diffusive evolution of the WMT anomaly in the Algerian basin (Borghini et al., 2014; Bryden, Schroeder, Borghini, et al., 2014) suggest that downward heat-salt fluxes along the local higher-gradient thermohalocline may be comparable to episodic large injections of dense waters; that is, diffusion would be much relevant than at our site. Neither are diffusive downward heat-salt fluxes homogeneous over time: saltier-warmer intermediate layers (LIW levels) since mid-2013 at the Minorca site yielded an increase in gradients of the thermohalocline and consequently in downward heat-salt fluxes (Figures 4a, 4b, 7b, and 7c). These observations are consistent with the progressive increment of  $\theta$  and  $S$  of the LIW overflowing the Sicily Channel since 2011 reported by Schroeder et al. (2017) and are of special interest since it may have important implications for the preconditioning of the water column in the GoL and therefore, for the new dense water formation.

## 5.2. Bulk Changes in the Deep Western Mediterranean: Heat, Salt, and Density

In a steady state ocean basin the downward diffusive transfer of heat and salt from the intermediate layers should be balanced by its removal through ventilation of the deep layers. The global ocean is currently out of equilibrium, gaining heat progressively for decades due to global warming (Cheng et al., 2019). During the early 21st century, the WMED has been markedly out of equilibrium, with the injection of ventilated waters adding heat and salt to the deep layers (rather than removing them) at a much higher rate than the continuous diffusive transfer.

Robust warming and salinification trends in the WMED deep waters have been reported for the twentieth century (e.g., Vargas-Yáñez et al., 2010) and diverse explanations of such trends have been discussed including atmospheric patterns (Rixen et al., 2005), modified properties of the AW entering through the Strait of Gibraltar (Millot, 2007) and changes in fresh water inputs due to river damming (Rohling & Bryden, 1992). Trends of around  $0.002\text{ }^{\circ}\text{C}/\text{year}$  for temperature and  $0.001\text{ year}^{-1}$  for salinity in the deep layers of the WMDW for the 1950–2000 period are accepted estimates (Vargas-Yáñez et al., 2009). When the WMT is added to the long-term series, temperature trends double ( $0.004\text{ }^{\circ}\text{C}/\text{year}$  [below 600 dbar], Vargas-Yáñez et al., 2017).

Although we rely on a single site time series, our trends are aligned with those of the overall WMED. Between 2004 and 2017  $\theta$  and  $S$  in the deep layers (1,280–2,420 dbar) off Minorca increased  $0.059\text{ }^{\circ}\text{C}$  and  $0.021$ , respectively, from which  $0.022\text{ }^{\circ}\text{C}$  and  $0.015$  occurred during 2004–2006 through the onset of the WMT. This abrupt rise added the equivalent of previous decadal increments in just 2 years. Linear trends for the 2007–2017 period (i.e., after the event) are similar to the long-term background salt-increase ( $0.001\text{ year}^{-1}$ ) but still higher for warming ( $0.003\text{ }^{\circ}\text{C}/\text{year}$ ).

Therefore, the effect of the WMT on the bulk changes of temperature and salinity of the deep WMED is outstanding. Translated into energy uptake, the 1,280–2,420 dbar layer in Minorca warming rate of  $\dot{Q} = 0.92\text{ W}/\text{m}^2$  (2005–2017) is more than two times that of the global intermediate ocean in the same period ( $0.4\text{ W}/\text{m}^2$ , 700–2,000 dbar, 2005–2016, Von Schuckmann et al., 2018). Such warming rate of the deep layers in the Western Mediterranean is even higher than the  $\dot{Q} \lesssim 0.7\text{ W}/\text{m}^2$  estimated for the upper 2,000 dbar in the global ocean in recent decades (Cheng et al., 2019; Von Schuckmann et al., 2018), indicating the relevance of the WMT as a case study of heat transfer into the deep ocean.

We have not considered so far the possible effect of geothermal heating on the evolution of the deep waters structure, however it is known to have a non-negligible contribution. Estimates of heat fluxes through the lithosphere in the WMED basin range between  $\dot{Q} \approx 0.05\text{ W}/\text{m}^2$  (Hofmann & Morales Maqueda, 2009) and  $\dot{Q} \approx 0.1\text{ W}/\text{m}^2$  (Davies & Davies, 2010), with slightly higher values for the more geothermally active

Tyrrhenian basin. Mean geothermal flux for the Algero-Provençal basin taken in Ferron et al. (2017) is  $\dot{Q} \approx 0.1 \text{ W/m}^2$ . This is about half of our estimation of downward diffusive heat flux during the 2005–2017 period. Geothermal heating was not included explicitly in the diffusion model since it is irregular in space and intermittent, so the inclusion of a fixed flux boundary condition at the seafloor would be arguable. Whatever the case, geothermal heating could account for up to 50% of the heat diffused from the intermediate layers into the deep waters. This extra heat coming across the seafloor should be removed from the budget assigned to lateral advection, that is, roughly speaking  $\dot{Q}$  would be shared as 0.6, 0.2 and  $0.1 \text{ W/m}^2$  for advection of ventilated waters, diffusion from the thermohalocline and geothermal heating respectively.

In addition to heat and salt increments, substantial changes were recorded in the density structure and stratification of the deep waters off Minorca. The onset of the WMT caused an increase in the potential density of the deep layers in just one year, inducing a strong stratification beneath the base of the thermohalocline (Figures 3 and 9a). After 2005, stratification was rapidly reduced to increase again with the arrival of new convective waters in the 2011–2013 period. Over the last years, deep-water density stabilized above 2004 values. Deep waters therefore show a quick stratification increase after major deep-water production events, followed by smooth stratification erosion afterward. Density and stratification of the deep waters play a major role in the formation rates of new deep waters, since they set the threshold for upper ocean densification. Deep water density levels higher than those pre-2005 hinder further deep-convection events. On the other hand, large periods when deep-water formation is absent will lighten the deep waters. Model projections suggest that the density of the deep waters formed in the WMED during the 21st century may be drastically reduced under a climate change scenario, leading to a sharp reduction in the formation rate of deep waters that penetrate below 1,000 m and consequently a weakening of the deep thermohaline circulation (Somot et al., 2006). Additionally, the recurrence of anomalous atmospheric patterns such as that of the extreme winter of 2005 is expected to increase due to global warming (Somavilla et al., 2016), so it seems likely that renewal of the deep WMED may be driven in the future by abrupt step-like shifts like the event that gave rise to the WMT.

### 5.3. Diffusive Mixing of the WMT Structure

Diffusive mixing was not dominant in the evolution of bulk *QC* and *SC* of the deep layers in Minorca, but it is a decisive agent in the overall evolution. Besides being the main driver in nonconvective periods, its action erodes the transient signals by homogenizing the water column, thus causing stratification to decrease relatively quickly. Simulations indicate that the signature of the extraordinary injection of 2005, without considering subsequent convective events, would need only 15 years to completely fade from the  $\theta$ - $S$  plane due to diffusive mixing.

The creation of the anomalous structure of 2005, showing distinct layers prone to the development of salt-fingering and diffusive layering, enabled us to run specific simulations based on state-of-the-art parameterizations and to infer a best guess of the general background turbulent diffusion coefficient due to processes not related to double-diffusion phenomena ( $K^\infty$ ). The obtained value of  $K^\infty = 4.25 \times 10^{-4} \text{ m}^2/\text{s}$  is an order of magnitude higher than those representative of the ocean interior (Thorpe, 2007; Zhang et al., 1998) but comparable to those typical of the abyssal ocean, especially in areas near seamounts or steep continental slopes (Waterhouse et al., 2014). Previous observational studies in the Mediterranean showed large spatial variability ranging from  $0.1\text{--}1 \times 10^{-4} \text{ m}^2/\text{s}$  for the deep waters in the abyssal plain between Sardinia and the Balearic Islands and much greater variability in certain areas such as the Ligurian Sea ( $1\text{--}3 \times 10^{-4} \text{ m}^2/\text{s}$ ), especially over the continental slope (Ferron et al., 2017). Cuypers et al. (2012) obtained estimated eddy diffusivity values ranging from  $0.1\text{--}10 \times 10^{-4} \text{ m}^2/\text{s}$  in the WMED basin below 1,500 dbar. Local  $K^\infty$  is estimated here from two periods, with four observations each, in which the thermohaline evolution is consistent with small or negligible advective contributions. Nevertheless, as stated before, diffusion and advection are not decoupled in the actual 3-D ocean. The implicit premise is that within each of these periods, the water column is homogeneous within the spatial advective scale. Since this is an arguable assumption, our  $K^\infty$  should be understood as a regional average which is in agreement with the upper limit of current estimates but is not necessarily as reliable as those emerging from specific ocean-mixing studies.

Treatment of double-diffusion processes considers specific terms to be added to an independent background  $K^\infty$ . Using parameterizations from Zhang et al. (1998) and Zhang and Schmitt (2000), we found a

satisfactory representation of the succession of mixing regimes and the asymmetries created in the mixing efficiency of heat and salt. Maximum transfer occurs at the base of the thermohalocline, where the greatest salt fingering activity was detected. Mean  $K_S = 5.8 \times 10^{-4} \text{ m}^2/\text{s}$  derived in the thermohalocline is similar to that estimated by Bryden, Schroeder, Borghini, et al. (2014) and Bryden, Schroeder, Sparnocchia, et al. (2014) from profiles in the Algerian basin at the same water column levels, although our mean  $K_\theta = 5.2 \times 10^{-4} \text{ m}^2/\text{s}$  is slightly higher.

An interesting feature within the WMT is the oWMDW-nWMDW interface at the base of the thermohalocline since it allows us to follow the spatio-temporal evolution of the anomaly (Schroeder et al., 2008, 2016) and to study the convergent effects of two different mixing phenomena. Upward fluxes due to diffusive layering below the interface supplement the downward transference of salt and heat due to the salt fingers above, causing an increase in  $\theta$  and  $S$  over time (Bryden, Schroeder, Borghini, et al., 2014). It is well known that diffusive layering is less effective than salt fingers in transferring heat and salt but the magnitude of the diffusive fluxes depends to a large extent on thermohaline gradients. Model runs indicate that for our WMT onset configuration the relative contribution of the diffusive layering to the evolution of salt in the interface during the first year of the anomaly represents up to 30%. By the end of 2008, diffusive layering was no longer operating effectively in the oWMDW-nWMDW region.

## 6. Conclusions

The onset of the WMT in 2005 created an unprecedented multilayered hydrographic structure in the deep ocean. The existence of a repeated hydrographic station, sampling this structure at seasonal frequency, enabled its evolution to be tracked for over 10 years until its almost complete erosion. The thermohaline evolution of the deep waters was understood as the combination of background diffusive mixing and intermittent advective renewals. Following this approach, a 1-D diffusion model sensitive to double-diffusion was set up in order to reproduce the hydrographic record. The exercise enabled us to show the large-scale specificities of double diffusion using current parametrizations of salt fingering and diffusive layering processes, to infer a regional background diffusivity value, and to describe the properties of the newly formed waters midway along their track from the formation area to the deepest part of the basin.

Two convective periods (2005–2006 and 2011–2013) account for most of the heat and salt gain of the deep water. Remarkably, heat uptake in the deep layers in the early 21st century period exceeds the estimated warming rate of the upper 2,000 dbar in the global ocean in the same period. After 12 years of evolution, the WMT hydrographic signature had been effectively eroded by the combined effect of the successive injections of dense waters and the diffusive mixing of their properties, yielding markedly warmer, saltier and slightly denser deep water than that present in the profiles prior to 2005. This may have a substantial impact on WMDW ventilation since the newly formed deep waters currently need to overcome a higher density threshold in order to penetrate to the deepest levels.

This study complements current knowledge of the WMT climatic event, as well as giving new insights into the mixing dynamics in the WMED interior. The data set and results presented here can be a useful tool to validate numerical simulations of deep-water formation. The importance of maintaining and expanding deep-water observatories such as the RADMED deep station in Minorca under a global change scenario should be highlighted. Finally, it is worth stressing the unique opportunity afforded by the formation of a well-defined interface in the deep ocean so as to understand the diffusive evolution in the ocean interior.

## Appendix A: Data assimilation in the model upper boundary

Data assimilation from the observed profiles in the upper boundary of the model is performed up to a pressure determined by an isopycnal depth that always remains above the oWMDW-nWMDW interface. Before estimating  $K_\theta$  and  $K_S$  profiles, at each  $\delta t$ ,

$$c(z, t) = c_{\text{casi}}(z, t) \cdot \gamma(z, t)^n + c_{\text{model}}(z, t) \cdot (1 - \gamma(z, t)^n), \quad z_{\text{min}} \leq z \leq z_{\text{max}}(t), \quad (\text{A1})$$

where  $c$  is the thermohaline tracer,  $z$  is the vertical coordinate,  $t$  is time,  $z_{\text{max}}$  is isopycnal pressure and the maximum pressure to assimilate,  $z_{\text{min}}$  is the minimum pressure of the simulation,  $c_{\text{model}}$  is the thermohaline tracer in the model and  $n$  controls the smoothness of the tracer assimilation in  $z_{\text{max}}$  ( $n = 4$  was used in this

study but since the diffusion equation (1) is solved by a second-order approximation, any correction above that order would be suitable).  $\gamma$  is defined as follows:

$$\gamma(z, t) = \frac{z_{\max}(t) - z}{z_{\max}(t) - z_{\min}}, \quad (\text{A2})$$

$z_{\max}$  is obtained from the observed profiles, for each  $\delta t$ :

$$z_{\max}(t) = (1 - \epsilon(t)) \cdot \sigma_i + \epsilon(t) \cdot \sigma_{i+1} \quad (\text{A3})$$

$$\epsilon(t) = \frac{t - i(t) \cdot \delta t - t_0}{\delta t} \quad (\text{A4})$$

$$i(t) = \left\lfloor \frac{t - t_0}{\delta t} \right\rfloor \quad (\text{A5})$$

where  $t_0$  corresponds to the initial time ( $t = 0$ ),  $i$  indexes the position of the first observed profile of the 15-day time window in which assimilation is taking place, and  $\sigma$  is the isopycnal pressure in the observed profile indexed by  $i$ .

The  $c_{\text{ass}}i$  term in equation (A1) is the thermohaline tracer profile to be assimilated obtained from the fortnightly time series ( $c_{\text{obs}}i$ ) indexed by  $i$ . It is obtained as follows:

$$c_{\text{ass}}i(z, t) = (1 - \epsilon(t)) \cdot c_{\text{obs}}i(z) + \epsilon(t) \cdot c_{\text{obs}}i+1(z). \quad (\text{A6})$$

#### Acknowledgments

This work was supported by the ATHAPOC project (CTM2014-54374-R), funded by Plan Nacional I+D+I and by the RADMED project, funded by the Instituto Español de Oceanografía. S. Piñeiro acknowledges the predoctoral FPI Fellowship (BES-2015-074316) support from the Spanish Ministry of Science, Innovation and Universities (MICINN), cofunded by the European Social Fund. The authors would like to thank the fieldwork and effort made by all the personnel involved in the RADMED surveys and especially M. Serra and J. L. López-Jurado. The authors are very grateful to the entire ATHAPOC group for their fruitful comments during the development of this work. Some of the instruments used during the cruises were made available by the Balearic Islands Coastal Observing and Forecasting System (ICTS-SOCIB), the Mediterranean Institute for Advanced Studies (IMEDEA CSIC-UIB), and the University of the Balearic Islands (UIB). The DoWEX experiment (<https://doi.org/10.17600/12450170>), part of the MERMEX program, and the BLUEFIN TUNA project, an ICTS-SOCIB and IEO joint research initiative, occupied the Minorca deep station in support of the RADMED monitoring program in 2012 and 2014, respectively. All the CTD casts used in this work can be accessed upon request at the SeaDataNet repository ([www.seadatanet.org](http://www.seadatanet.org)).

#### References

- Barker, P. M., & McDougall, T. J. (2017). Stabilizing hydrographic profiles with minimal change to the water masses. *Journal of Atmospheric and Oceanic Technology*, 34(9), 1935–1945. <https://doi.org/10.1175/JTECH-D-16-0111.1>
- Bethoux, J. P., Durrieu de Madron, X., Nyffeler, F., & Tailliez, D. (2002). Deep water in the Western Mediterranean: Peculiar 1999 and 2000 characteristics, shelf formation hypothesis, variability since 1970 and geochemical inferences. *Journal of Marine Systems*, 33–34, 117–131. [https://doi.org/10.1016/S0924-7963\(02\)00055-6](https://doi.org/10.1016/S0924-7963(02)00055-6)
- Bethoux, J. P., & Tailliez, D. (1994). Deep-water in the Western Mediterranean Sea, yearly climatic signature and enigmatic spreading, (1st ed.). In P. Malanotte-Rizzoli, & A. R. Robinson (Eds.), *Ocean processes in climate dynamics: Global and Mediterranean examples* (pp. 355–369). Dordrecht: Springer Netherlands. <https://doi.org/10.1007/978-94-011-0870-6-15>
- Beuvier, J., Béranger, K., Brossier, C. L., Somot, S., Sevault, F., Drillet, Y., & Lyard, F. (2012). Spreading of the Western Mediterranean deep water after winter 2005: Time scales and deep cyclone transport. *Journal of Geophysical Research*, 117, C07022. <https://doi.org/10.1029/2011JC007679>
- Bindoff, N. L., & McDougall, T. J. (1994). Diagnosing climate change and ocean ventilation using hydrographic data. *Journal of Physical Oceanography*, 24(6), 1137–1152. [https://doi.org/10.1175/1520-0485\(1994\)024<1137:DCCAOV>2.0.CO;2](https://doi.org/10.1175/1520-0485(1994)024<1137:DCCAOV>2.0.CO;2)
- Borghini, M., Bryden, H. L., Schroeder, K., Sparnocchia, S., & Vetrano, A. (2014). The Mediterranean is becoming saltier. *Ocean Science*, 10, 693–700. <https://doi.org/10.5194/os-10-693-2014>
- Bryden, H. L., Schroeder, K., Borghini, M., Vetrano, A., & Sparnocchia, S. (2014). Mixing in the deep waters of the Western Mediterranean, *The Mediterranean Sea: Temporal variability and spatial patterns* (pp. 51–58). Oxford: John Wiley and Sons Inc. <https://doi.org/10.1002/9781118847572>
- Bryden, H. L., Schroeder, K., Sparnocchia, S., Borghini, M., & Vetrano, A. (2014). Thermohaline staircases in the Western Mediterranean Sea. *Journal of Marine Research*, 72(1), 1–18. <https://doi.org/10.1357/002224014812655198>
- Canals, M., Puig, P., Durrieu de Madron, X., Heussner, S., Palanques, A., & Fabres, J. (2006). Flushing submarine canyons. *Nature*, 444(7117), 354–357. <https://doi.org/10.1038/nature05271>
- Cheng, L., Abraham, J., Hausfather, Z., & Trenberth, K. E. (2019). How fast are the oceans warming? *Science*, 363(6423), 128–129. <https://doi.org/10.1126/science.aav7619>
- Chiggiato, J., Schroeder, K., & Trincardi, F. (2016). Cascading dense shelf-water during the extremely cold winter of 2012 in the Adriatic, Mediterranean Sea: Formation, flow, and seafloor impact. *Marine Geology*, 375, 1–4. <https://doi.org/10.1016/j.margeo.2016.03.002>
- Conan, P., Testor, P., Estournel, C., D'Ortenzio, F., Pujo-Pay, M., & Durrieu de Madron, X. (2018). Preface to the special section: Dense water formations in the northwestern Mediterranean: From the physical forcings to the biogeochemical consequences. 6983–6995, 123. <https://doi.org/10.1029/2018JC014301>
- Crank, J., & Nicolson, P. (1947). A practical method for numerical evaluation of solutions of partial differential equations of the heat-conduction type. *Mathematical Proceedings of the Cambridge Philosophical Society*, 43(1), 50–67. <https://doi.org/10.1017/S0305004100023197>

- Cuypers, Y., Bouruet-Aubertot, P., Marec, C., & Fuda, J. L. (2012). Characterization of turbulence from a fine-scale parameterization and microstructure measurements in the Mediterranean Sea during the BOUM experiment. *Biogeosciences*, *9*(8), 3131–3149. <https://doi.org/10.5194/bg-9-3131-2012>
- Davies, J. H., & Davies, D. R. (2010). Earth's surface heat flux. *Solid Earth*, *1*(1), 5–24. <https://doi.org/10.5194/se-1-5-2010>
- de Boer, G. J., Pietrzak, J. D., & Winterwerp, J. C. (2008). Using the potential energy anomaly equation to investigate tidal straining and advection of stratification in a region of freshwater influence. *Ocean Modelling*, *22*, 1–11. <https://doi.org/10.1016/j.ocemod.2007.12.003>
- Durante, S., Schroeder, K., Mazzei, L., Pierini, S., Borghini, M., & Sparnocchia, S. (2019). Permanent thermohaline staircases in the Tyrrhenian Sea. *Geophysical Research Letters*, *46*, 1562–1570. <https://doi.org/10.1029/2018GL081747>
- Durrieu de Madron, X., Houpert, L., Puig, P., Sanchez-Vidal, A., Testor, P., Bosse, A., & Raimbault, P. (2013). Interaction of dense shelf water cascading and open-sea convection in the northwestern Mediterranean during winter 2012. *Geophysical Research Letters*, *40*, 1379–1385. <https://doi.org/10.1002/grl.50331>
- Durrieu de Madron, X., Ramondenc, S., Berline, L., Houpert, L., Bosse, A., Martini, S., & ANTARES collaboration (2017). Deep sediment resuspension and hick nepheloid layer generation by open-ocean convection. *Journal of Geophysical Research: Oceans*, *122*, 2291–2318. <https://doi.org/10.1002/2016JC012062>
- Emery, W. J., & Thomson, R. E. (2001). *Data analysis methods in physical oceanography*. Oxford: Elsevier Science & Technology.
- Ferron, B., Bouruet-Aubertot, P., Cuypers, Y., Schroeder, K., & Borghini, M. (2017). How important are diapycnal mixing and geothermal heating for the deep circulation of the Western Mediterranean? *Geophysical Research Letters*, *44*, 7845–7854. <https://doi.org/10.1002/2017GL074169>
- Font, J., Puig, P., Salat, J., & Palanques, A. (2007). Sequence of hydrographic changes in NW Mediterranean deep water due to the exceptional winter of 2005. *Scientia Marina*, *71*(2), 339–346. <https://doi.org/10.3989/scimar.2007.71n2339>
- Fuda, J. L., Bengara, L., Ismail, S. B., Curtil, C., Moumni, B. E., Font, J., & Tamburini, C. (2009). Recent dense water formation in the Med western basin, as observed by HYDROCHANGES, *CIESM workshop monographs* pp. 29–33. Monaco: CIESM.
- García-Lafuente, J., Delgado, J., Sánchez-Román, A., Soto, J., Carracedo, L., & Díaz del Río, G. (2009). Interannual variability of the Mediterranean outflow observed in Espartel sill, western Strait of Gibraltar. *Journal of Geophysical Research*, *114*, C10018. <https://doi.org/10.1029/2009JC005496>
- Hofmann, M., & Morales Maqueda, M. A. (2009). Geothermal heat flux and its influence on the oceanic abyssal circulation and radiocarbon distribution. *Geophysical Research Letters*, *36*, L03603. <https://doi.org/10.1029/2008GL036078>
- Houpert, L., Durrieu de Madron, X., Testor, P., Bosse, A., D'Ortenzio, F., Bouin, M. N., & Raimbault, P. (2016). Observations of open-ocean deep convection in the northwestern Mediterranean Sea: Seasonal and interannual variability of mixing and deep water masses for the 2007–2013 period. *Journal of Geophysical Research: Oceans*, *121*, 8139–8171. <https://doi.org/10.1002/2016JC011857>
- IOC, SCOR, & IAPSO (2010). The international thermodynamic equation of seawater 2010: Calculation and use of thermodynamic properties. (No. June) UNESCO.
- Jayne, S. R. (2009). The impact of abyssal mixing parameterizations in an ocean general circulation model. *Journal of Physical Oceanography*, *39*(7), 1756–1775. <https://doi.org/10.1175/2009JPO4085.1>
- Johannessen, O. M., & Lee, O. S. (1974). A deep stepped thermo-haline structure in the Mediterranean. *Deep-Sea Research and Oceanographic Abstracts*, *21*(8), 629–639. [https://doi.org/10.1016/0011-7471\(74\)90047-3](https://doi.org/10.1016/0011-7471(74)90047-3)
- Kelley, D. E. (1984). Effective diffusivities within oceanic thermohaline staircases. *Journal of Geophysical Research*, *89*(11), 484–488.
- Kelley, D. E. (1990). Fluxes through diffusive staircases: A new formulation. *Journal of Geophysical Research*, *95*(C3), 3365–3371. <https://doi.org/10.1029/JC095iC03p03365>
- Kelley, D. E., Fernando, H. J. S., Gargett, A. E., Tanny, J., & Özsoy, E. (2003). The diffusive regime of double-diffusive convection. *Progress in Oceanography*, *56*(3-4), 461–481. [https://doi.org/10.1016/S0079-6611\(03\)00026-0](https://doi.org/10.1016/S0079-6611(03)00026-0)
- Klymak, J., & Nash, J. D. (2009). Estimates of mixing, (2nd ed.). *Encyclopedia of ocean sciences* (Vol. 2, pp. 288–298). London: Elsevier Ltd. <https://doi.org/10.1016/B978-012374473-9.00615-9>
- Kunze, E., & Toole, J. M. (1997). Tidally driven vorticity, diurnal shear, and turbulence atop Fieberling Seamount. *Journal of Physical Oceanography*, *27*(12), 2663–2693. [https://doi.org/10.1175/1520-0485\(1997\)027<2663:TDVDSA>2.0.CO;2](https://doi.org/10.1175/1520-0485(1997)027<2663:TDVDSA>2.0.CO;2)
- Lacombe, H., Tchernia, P., & Gamberoni, L. (1985). Variable bottom water in the Western Mediterranean basin. *Progress in Oceanography*, *14*(C), 319–338. [https://doi.org/10.1016/0079-6611\(85\)90015-1](https://doi.org/10.1016/0079-6611(85)90015-1)
- Ledwell, J. R., Montgomery, E. T., Polzin, K. L., St. Laurent, L. C., Schmitt, R. W., & Toole, J. M. (2000). Evidence for enhanced mixing over rough topography in the abyssal ocean. *Nature*, *403*(6766), 179–182. <https://doi.org/10.1038/35003164>
- Ledwell, J. R., Watson, A. J., & Law, C. S. (1993). Evidence for slow mixing across the pycnocline from an open-ocean tracer-release experiment. *Nature*, *364*(6439), 701–703. <https://doi.org/10.1038/364701a0>
- Ledwell, J. R., Watson, A. J., & Law, C. S. (1998). Mixing of a tracer in the pycnocline. *Journal of Geophysical Research*, *103*(C10), 21,499–21,529. <https://doi.org/10.1029/98JC01738>
- López-Jurado, J. L., Balbín, R., Alemany, F., Amengual, B., Aparicio-González, A., Fernandez de Puelles, M. L., & Vargas-Yáñez, M. (2015). The RADMED monitoring programme as a tool for MSFD implementation: Towards an ecosystem-based approach. *Ocean Science*, *11*, 897–908. <https://doi.org/10.5194/os-11-897-2015>
- López-Jurado, J. L., González-Pola, C., & Vélez-Belchí, P. (2005). Observation of an abrupt disruption of the long-term warming trend at the Balearic Sea, Western Mediterranean Sea, in summer 2005. *Geophysical Research Letters*, *32*, L24606. <https://doi.org/10.1029/2005GL024430>
- MEDOC Group (1970). Observation of formation of deep water in the Mediterranean Sea. *Nature*, *227*, 1037–1040.
- Marshall, J., & Schott, F. (1999). Open-ocean convection: Observations, theory and models. *Reviews of Geophysics*, *37*(98), 1–64. <https://doi.org/10.1029/98RG02739>
- Meccia, V., Simoncelli, S., & Sparnocchia, S. (2016). Decadal variability of the Turner angle in the Mediterranean Sea and its implications for double diffusion. *Deep-Sea Research Part I: Oceanographic Research Papers*, *114*, 64–77. <https://doi.org/10.1016/j.dsr.2016.04.001>
- Millot, C. (2007). Interannual salinification of the Mediterranean inflow. *Geophysical Research Letters*, *34*, L21609. <https://doi.org/10.1029/2007GL031179>
- Onken, R. (2003). Double diffusion in the Mediterranean Sea: Observation and parameterization of salt finger convection. *Journal of Geophysical Research*, *108*(C9), 8124. <https://doi.org/10.1029/2002JC001349>
- Planque, B., Lazure, P., & Jegou, A. (2006). Typology of hydrological structures modelled and observed over the Bay of Biscay shelf. *Scientia Marina*, *70*(June), 43–50. <https://doi.org/10.3989/scimar.2006.70s143>
- Polzin, K. L., Toole, J. M., Ledwell, J. R., & Schmitt, R. W. (1997). Spatial variability of turbulent mixing in the abyssal ocean. *Science*, *276*(5309), 93–96. <https://doi.org/10.1126/science.276.5309.93>

- Puig, P., Durrieu de Madron, X., Salat, J., Schroeder, K., Martín, J., Karageorgis, A. P., & Houpert, L. (2013). Thick bottom nepheloid layers in the Western Mediterranean generated by deep dense shelf water cascading. *Progress in Oceanography*, *111*, 1–23. <https://doi.org/10.1016/j.pocean.2012.10.003>
- Puig, P., Palanques, A., Font, J., Salat, J., Latasa, M., & Scharek, R. (2009). Interactions between open-sea convection and shelf cascading dense waters in the formation of the Western Mediterranean deep water. *CIESM workshop monographs* pp. 81–89). Monaco: CIESM.
- Radko, T. (2013). *Double-diffusive convection* (1st ed.). New York: Cambridge University Press.
- Rhein, M. (1995). Deep water formation in the Western Mediterranean. *Journal of Geophysical Research*, *100*(C4), 6943–6959. <https://doi.org/10.1029/94JC03198>
- Rixen, M., Beckers, J. M., Levitus, S., Antonov, J., Boyer, T., Maillard, C., & Zavatarelli, M. (2005). The Western Mediterranean deep water: A proxy for climate change. *Geophysical Research Letters*, *32*, L12608. <https://doi.org/10.1029/2005GL022702>
- Rohling, E. J., & Bryden, H. L. (1992). Man-induced salinity and temperature increases in Western Mediterranean deep water. *Journal of Geophysical Research*, *97*(C7), 11,191–11,198. <https://doi.org/10.1029/92JC00767>
- Ruddick, B. (1983). A practical indicator of the stability of the water column to double-diffusive activity. *Deep Sea Research Part A, Oceanographic Research Papers*, *30*(10), 1105–1107. [https://doi.org/10.1016/0198-0149\(83\)90063-8](https://doi.org/10.1016/0198-0149(83)90063-8)
- Salat, J., Emelianov, M., & López-Jurado, J. L. (2007). Atypical Western Mediterranean deep water formation during winter 2005. *Rapport du Commission Internationale de la Mer Méditerranée*, *38* (pp. 197). Istanbul: CIESM.
- Salat, J., Emelianov, M., & Puig, P. (2009). From bottom water (Lacombe, 1985) to New-WMDW since 2005. Possible shifts on open sea deep convection. *CIESM workshop monographs* (pp. 41–49). Monaco: CIESM.
- Schmitt, R. W. (1994). Double diffusion in oceanography. *Annual Review of Fluid Mechanics*, *26*, 255–285. <https://doi.org/10.1146/annurev.fl.26.010194.001351>
- Schmitt, R. W. (2009). Double-diffusive convection, (2nd ed.), *Encyclopedia of ocean sciences* (Vol. 2, pp. 162–170). London: Elsevier Ltd.
- Schmitt, R. W., & Ledwell, J. R. (2001). Dispersion and diffusion in the deep ocean, (1st ed.). *Encyclopedia of ocean sciences* (Vol. 2, pp. 726–733). London: Elsevier Ltd. <https://doi.org/10.1006/rwos.2001.0137>
- Schmitt, R. W., Ledwell, J. R., Montgomery, E. T., Polzin, K. L., & Toole, J. M. (2005). Enhanced diapycnal mixing by salt fingers in the thermocline of the tropical Atlantic. *Science*, *308*(5722), 685–688. <https://doi.org/10.1126/science.1108678>
- Schroeder, K., Chiggiato, J., Bryden, H. L., Borghini, M., & Ismail, S. B. (2016). Abrupt climate shift in the Western Mediterranean Sea. *Nature Scientific Reports*, *6*, 23009. <https://doi.org/10.1038/srep23009>
- Schroeder, K., Chiggiato, J., Josey, S. A., Borghini, M., Aracri, S., & Sparnocchia, S. (2017). Rapid response to climate change in a marginal sea. *Scientific Reports*, *7*(1), 1–7. <https://doi.org/10.1038/s41598-017-04455-5>
- Schroeder, K., Gasparini, G. P., Borghini, M., & Ribotti, A. (2009). Experimental evidence of recent abrupt changes in the deep Western Mediterranean Sea. *CIESM workshop monographs* (pp. 51–56). Monaco: CIESM.
- Schroeder, K., Gasparini, G. P., Tangherlini, M., & Astraldi, M. (2006). Deep and intermediate water in the Western Mediterranean under the influence of the eastern Mediterranean transient. *Geophysical Research Letters*, *33*(21), L21607. <https://doi.org/10.1029/2006GL027121>
- Schroeder, K., Josey, S. A., Herrmann, M., Grignon, L., Gasparini, G. P., & Bryden, H. L. (2010). Abrupt warming and salting of the Western Mediterranean deep water after 2005: Atmospheric forcings and lateral advection. *Journal of Geophysical Research*, *115*, C08029. <https://doi.org/10.1029/2009JC005749>
- Schroeder, K., Millot, C., Bengara, L., Ben Ismail, S., Bensi, M., Borghini, M., & Vetrano, A. (2013). Long-term monitoring programme of the hydrological variability in the Mediterranean Sea: A first overview of the HYDROCHANGES network. *Ocean Science*, *9*(2), 301–324. <https://doi.org/10.5194/os-9-301-2013>
- Schroeder, K., Ribotti, A., Borghini, M., Sorgente, R., Perilli, A., & Gasparini, G. P. (2008). An extensive Western Mediterranean deep water renewal between 2004 and 2006. *Geophysical Research Letters*, *35*, L18605. <https://doi.org/10.1029/2008GL035146>
- Seifert, B., & Gasser, T. (2004). Local polynomial smoothing (2nd ed.). In S. Kotz, N. Balakrishnan, C. B. Read, B. Vidakovic, & N. L. Johnson (Eds.), *Encyclopedia of statistical sciences*, *7* pp. 4334–4339). Hoboken, New Jersey: John Wiley and Sons Inc. <https://doi.org/10.1002/0471667196.ess0672.pub2>
- Smith, R. O., Bryden, H. L., & Stansfield, K. (2008). Observations of new Western Mediterranean deep water formation using Argo floats 2004–2006. *Ocean Sciences*, *4*, 133–149. <https://doi.org/10.5194/os-4-133-2008>
- Somavilla, R., González-Pola, C., Schauer, U., & Budéus, G. (2016). Mid-2000s North Atlantic shift: Heat budget and circulation changes. *Geophysical Research Letters*, *43*, 2059–2068. <https://doi.org/10.1002/2015GL067254>
- Somot, S., Houpert, L., Sevault, F., Testor, P., Bosse, A., Taupier-Letage, I., & Herrmann, M. (2018). Characterizing, modelling and understanding the climate variability of the deep water formation in the north-western Mediterranean Sea. *Climate Dynamics*, *51*(3), 1179–1210. <https://doi.org/10.1007/s00382-016-3295-0>
- Somot, S., Sevault, F., & Déqué, M. (2006). Transient climate change scenario simulation of the Mediterranean Sea for the twenty-first century using a high-resolution ocean circulation model. *Climate Dynamics*, *27*(7–8), 851–879. <https://doi.org/10.1007/s00382-006-0167-z>
- St. Laurent, L. C., & Schmitt, R. W. (1999). The contribution of salt fingers to vertical mixing in the North Atlantic Tracer Release Experiment\*. *Journal of Physical Oceanography*, *29*(7), 1404–1424. [https://doi.org/10.1175/1520-0485\(1999\)029<1404:TCOSFT>2.0.CO;2](https://doi.org/10.1175/1520-0485(1999)029<1404:TCOSFT>2.0.CO;2)
- St. Laurent, L. C., Toole, J. M., & Schmitt, R. W. (2001). Buoyancy forcing by turbulence above rough topography in the abyssal Brazil basin. *Journal of Physical Oceanography*, *31*(12), 3476–3495. [https://doi.org/10.1175/1520-0485\(2001\)031<3476:FBFTAR>2.0.CO;2](https://doi.org/10.1175/1520-0485(2001)031<3476:FBFTAR>2.0.CO;2)
- Thorpe, S. A. (2007). *An introduction to ocean turbulence* (1st ed.). Cambridge University Press.
- Toole, J. M., Polzin, K. L., & Schmitt, R. W. (1994). Estimates of diapycnal mixing in the abyssal ocean. *Science*, *264*, 1992–1995.
- Turner, J. S. (1973). *Buoyancy effects in fluids*. London: Cambridge University Press.
- Vargas-Yáñez, M., García-Martínez, M. C., Moya, F., Balbín, R., López-Jurado, J. L., Serra, M., & Salat, J. (2017). Updating temperature and salinity mean values and trends in the Western Mediterranean: The RADMED project. *Progress in Oceanography*, *157*(August), 27–46. <https://doi.org/10.1016/j.pocean.2017.09.004>
- Vargas-Yáñez, M., Moya, F., García-Martínez, M. C., Tel, E., Zunino, P., Plaza, F., & Serra, M. (2010). Climate change in the Western Mediterranean Sea 1900–2008. *Journal of Marine Systems*, *82*(3), 171–176. <https://doi.org/10.1016/j.jmarsys.2010.04.013>
- Vargas-Yáñez, M., Moya, F., Tel, E., García-Martínez, M. C., Guerber, E., & Bourgeon, M. (2009). Warming and salting in the Western Mediterranean during the second half of the 20th century: Inconsistencies, unknowns and the effect of data processing. *Scientia Marina*, *73*(1), 7–28. <https://doi.org/10.3989/scimar.2009.73n1007>

- Von Schuckmann, K., Storto, A., Simoncelli, S., Roshin P, R., Samuelsen, A., de Pascual Collar, A., & Szerkely, T. (2018). Ocean heat content, *Copernicus Service ocean state report, 2* (pp. s41–s45). *Journal of Operational Oceanography*, 11 <https://doi.org/10.1080/1755876X.2018.1489208>
- Waldman, R., Somot, S., Herrmann, M., Testor, P., Estournel, C., Sevault, F., & Dausse, D.(2016). Estimating dense water volume and its evolution for the year 2012–2013 in the Northwestern Mediterranean Sea: An observing system simulation experiment approach. *Journal of Geophysical Research: Oceans*, 121, 6696–6716. <https://doi.org/10.1002/2016JC011694>
- Waterhouse, A. F., MacKinnon, J. A., Nash, J. D., Alford, M. H., Kunze, E., Simmons, H. L., & Lee, C. M. (2014). Global patterns of diapycnal mixing from measurements of the turbulent dissipation rate. *Journal of Physical Oceanography*, 44(7), 1854–1872. <https://doi.org/10.1175/JPO-D-13-0104.1>
- Winton, M., Griffies, S. M., Samuels, B. L., Sarmiento, J. L., & Frölicher, T. L. (2013). Connecting changing ocean circulation with changing climate. *Journal of Climate*, 26(7), 2268–2278. <https://doi.org/10.1175/JCLI-D-12-00296.1>
- Zhang, J., & Schmitt, R. W. (2000). The impact of salt fingering on the thermohaline circulation under mixed boundary conditions. *Journal of Physical Oceanography*, 30(6), 1223–1231. [https://doi.org/10.1175/1520-0485\(2000\)030<1223:TIOSFO>2.0.CO;2](https://doi.org/10.1175/1520-0485(2000)030<1223:TIOSFO>2.0.CO;2)
- Zhang, J., Schmitt, R. W., & Huang, R. X. (1998). Sensitivity of the GFDL Modular Ocean Model to parameterization of double-diffusive processes. *Journal of Physical Oceanography*, 28(4), 589–605. [https://doi.org/10.1175/1520-0485\(1998\)028<0589:SOTGMO>2.0.CO;2](https://doi.org/10.1175/1520-0485(1998)028<0589:SOTGMO>2.0.CO;2)
- Zodiatis, G., & Gasparini, G. P. (1996). Thermohaline staircase formations in the Tyrrhenian Sea. *Deep-Sea Research Part I: Oceanographic Research Papers*, 43(5), 655–678. [https://doi.org/10.1016/0967-0637\(96\)00032-5](https://doi.org/10.1016/0967-0637(96)00032-5)
- Zunino, P., Schroeder, K., Vargas-yáñez, M., Gasparini, G. P., & Coppola, L. (2012). Effects of the Western Mediterranean Transition on the resident water masses: Pure warming, pure freshening and pure heaving. *Journal of Marine Systems*, 96-97, 15–23. <https://doi.org/10.1016/j.jmarsys.2012.01.011>